

In Situ Absorption and Fluorescence Microspectroscopy Investigation of the Molecular Incorporation Process into Single Nanoporous Protein Crystals

Takayuki Uwada,* Kohei Kouno, and Mitsuru Ishikawa



Cite This: *ACS Omega* 2020, 5, 9605–9613



Read Online

ACCESS |



Metrics & More

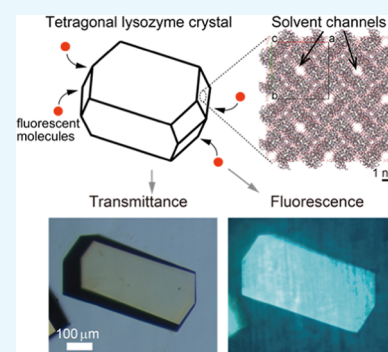


Article Recommendations



Supporting Information

ABSTRACT: Protein crystals exhibit distinct three-dimensional structures, which contain well-ordered nanoporous solvent channels, providing a chemically heterogeneous environment. In this paper, the incorporation of various molecules into the solvent channels of native hen egg-white lysozyme crystals was demonstrated using fluorescent dyes, including acridine yellow G, rhodamine 6G, and eosin Y. The process was evaluated on the basis of absorption and fluorescence microspectroscopy at a single-crystal level. The molecular loading process was clearly visualized as a function of time, and it was determined that the protein crystals could act as nanoporous materials. It was found that the incorporation process is strongly dependent on the molecular charge, leading to heterogeneous molecular aggregation, which suggests host–guest interaction of protein crystals from the viewpoint of nanoporous materials.



INTRODUCTION

Protein crystals have predominantly been studied utilizing X-ray crystallography techniques to establish their molecular structures. It is known that proteins exhibit distinct three-dimensional structures, which contain well-ordered nanoporous solvent channels, usually 0.5–10 nm in diameter. These channels are typically filled with water molecules, which constitute a large proportion of the crystal volume and display remarkably high internal surface areas.^{1–3} From this viewpoint, structural similarities to nanoporous materials, such as zeolite,⁴ mesoporous silica,⁵ and metal–organic frameworks (MOFs), are noteworthy.⁶ It is expected that similarly to MOFs, protein crystals will be employed in a broader range of applications, including molecular sieves, catalysis, and drug delivery systems. Nevertheless, protein crystals have limitations, which mainly result from their mechanical and chemical fragility. It has been proposed that protein crystals can be easily stabilized by the addition of covalent bonds between neighboring proteins, i.e., chemical cross-linking. The method for producing cross-linked crystals is already particularly established for protein hen egg-white lysozyme (HEWL) and involves soaking the crystals in a glutaraldehyde solution.^{7,8} The crystals are robust with respect to temperature, acid, base, or solvent changes, and their potential applications are widely investigated.

Among various applications, synthesis of nanomaterials using protein crystals has recently gained significant attention. Such approaches are primarily based on the cross-linked HEWL crystals. The solvent channels in protein crystals can provide a chemically heterogeneous and confined environment and are expected to be used as synthesis templates. In other

words, these materials exhibit crystalline scaffolds analogous to those of nanomaterials. For example, Mann et al. synthesized gold and silver nanoparticles by soaking protein crystals in an aqueous solution of a metal salt and a reducing agent.^{9,10} The same group also succeeded in the preparation of luminescent carbon dots using the same approach.¹¹ On the other hand, Ueno et al. reported the synthesis of CoPt nanoparticles and described the controlling of the magnetic properties of the materials by utilizing different crystalline phases.¹² Moreover, Zhang and co-workers assembled lanthanide complexes in protein solvent channels by mixing with the component solution of organic solvents.¹³ All of these results demonstrate the potential of protein crystals as templates for the synthesis of nanomaterials and suggest that molecules or ions can diffuse into protein crystals from solution. However, the molecular incorporation into the crystals was supported as the result of the obtained product. This implies that the dynamic process of a chemical synthesis in the protein crystals from the material incorporation into the product is not well understood, especially the spatial distribution of the materials. Moreover, the interaction between the incorporated materials and the surface of the nanopores of the protein crystals, i.e., the host–guest interaction, has not been sufficiently examined. Because

Received: March 7, 2020

Accepted: April 2, 2020

Published: April 17, 2020



protein molecules possess a net charge, which is affected by the pH of their surrounding environment, the possible electrostatic interactions should be further evaluated. Furthermore, the study of protein crystals as nanoporous materials is a largely unexplored area in comparison with the synthetic chemistry counterparts.

Considering the intriguing properties of protein crystals as nanoporous materials, several research groups have described the molecular incorporation into protein crystals, both theoretically and experimentally.^{2,14–21} For instance, Farhadian et al. used theoretical methods to predict that glycine molecules can diffuse into HEWL crystals via solvent channels and would be trapped near the entrances by lysine, arginine, and aspartic acid residues.¹⁴ In addition, Guli and co-workers demonstrated loading of bromophenol blue into cross-linked HEWL crystals. Using diffuse reflectance spectroscopy, the group revealed that the absorption spectra of crystalline powder samples exhibited a red shift in comparison to that of the bulk solution, implying a confinement effect within the channels.¹⁵ The host–guest interaction has been suggested; however, it is still not fully understood. Powder samples result in aggregates such as dimers formed on the external surfaces of crystals, which drastically affect spectral shapes.

An important work in this field was performed by Cvetkovic et al. The group focused on evaluating molecular loading properties of native and cross-linked HEWL crystals of different morphologies and examined them by loading fluorescent molecules into the crystals.^{16–19} It should be noted that the methodology was developed based on measurements of collective crystals to single ones, utilizing loading of fluorescent molecules and analyzing the materials using confocal fluorescence microscopy. The single-crystal imaging elucidated the dynamic process of molecular loading into the crystals, depending on the channel size and the molecular diffusion anisotropy. Although better insight into the protein crystals as nanoporous materials was obtained by their work, understanding the host–guest interaction remained unaddressed. Hence, spectroscopic analysis of the loaded molecules in the protein crystals is essential. From this viewpoint, Kuhn's group also employed confocal and two-photon excited fluorescence microscopy and examined the pH and Ca^{2+} ion concentration inside single HEWL crystals by introducing pH-sensitive fluorescent molecules into the crystals.^{20,21} They demonstrated that the fluorescence image exhibited spatial distribution of pH inside the single crystals. Moreover, it was shown that space-resolved spectroscopy allows for sensitive detection. These outcomes further indicate that the observation of the loading of guest molecules into single protein crystals and their distribution using not just imaging but also spectroscopic approaches is required to obtain a comprehensive understanding of the host–guest interaction, including the position dependence.

In this study, we conducted an optical microscopy investigation on the diffusion and distribution of fluorescent dyes in HEWL crystals at a single-crystal level. We also thoroughly examined the host–guest interactions, utilizing the space-resolved absorption and fluorescence spectroscopy analyses conducted using an optical microscope. We immersed the already-prepared HEWL crystals into a fluorescence dye buffer solution containing the lysozyme and conducted an evaluation of the crystals under an optical microscope. In addition, we employed fluorescent dyes with various charges to investigate whether the charge of the guest species has an effect

on the penetration of the molecules into the solvent channels and the interaction with the charge of the channel surface. In this study, the primary focus involved the native HEWL crystals because the molecular loading process into crystals of this type is remarkably simple. A better understanding of the native protein crystals as nanoporous materials is essential, and it is hoped that the outcomes of our study will provide a platform for the examination of the effects of cross-linking.

EXPERIMENTAL SECTION

Protein Crystal Preparation. Hen egg-white lysozyme was purchased from Sigma-Aldrich and used without further purification. HEWL was crystallized employing the vapor diffusion method using 48-well crystallization plates (HR3-179, Hampton Research). Briefly, 7 μL of 50 mg/mL HEWL dissolved in a 0.1 M sodium acetate buffer solution (pH 4.5) and 7 μL of 0.1 M NaCl in a 0.1 M sodium acetate buffer solution were added to each well. NaCl was used as a precipitant, and the solution in the well was the “mother solution”. Subsequently, 200 μL of 0.1 M NaCl in a 0.1 M sodium acetate solution was poured into each reservoir. The plate was then sealed with a transparent sealing film (HR3-609, Hampton Research) and incubated at 20 °C. The crystal growth progress was followed using a stereoscopic microscope (SZ61TR, Olympus). After 72 h, grown HEWL crystals (~hundreds of micrometer in length) were obtained. Based on the microscopic observation, the crystal shapes could be divided into two groups, hexagonal and square-shaped, as presented in Figure 1a,b, respectively. These can be assigned to

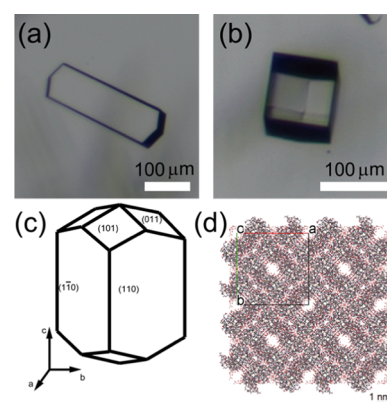


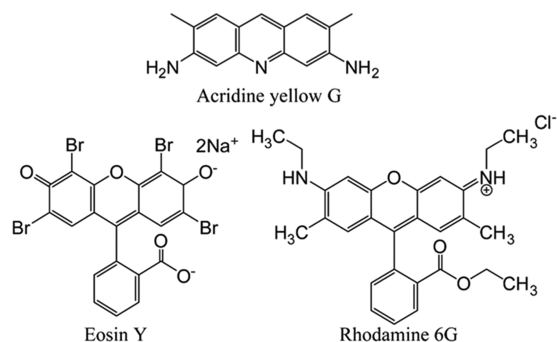
Figure 1. Transmittance microscopic images of hen egg-white lysozyme crystals obtained using the above experimental procedure. The (a) hexagonal and (b) square-shaped ones correspond to (110) and (101) faces of the tetragonal HEWL crystals, respectively. (c) Schematic illustration of the morphology of a tetragonal HEWL crystal, showing the crystallographic axes and faces. (d) *c*-axis projection of the structure of the tetragonal HEWL crystal.

(110) and (101) faces of the tetragonal HEWL crystals, respectively (Figure 1c).^{22,23} The tetragonal crystals contain solvent channels along with the *c*-axis as presented in Figure 1d, whereas obvious channels are not found along with the *a*- and *b*-axis (Figure S1). The crystal structure was imported from the Protein Data Bank (PDB code 193L)²⁴ into the Mercury software.

Molecular Incorporation. Molecular loading into the HEWL crystals was performed using the following procedure. The sealing film was initially peeled off from the crystallization plate, and 7 μL of various concentrations of the dye in a

sodium acetate buffer solution was added to the well containing HEWL crystals. Subsequently, the plate was sealed again and placed under an inverted microscope for optical measurement. Notably, HEWL was mixed with the dye solution (50 mg/mL) to avoid crystal dissolution, owing to decreasing concentration. The dye types employed in this study are provided in Chart 1. Acridine yellow G was purchased from Sigma-Aldrich, whereas eosin Y and rhodamine 6G were obtained from Wako Chemical and used without further purification.

Chart 1. Structures of Fluorescent Dye Molecules Incorporated in Hen Egg-White Lysozyme Crystals



Optical Measurement. Transmittance (absorption) and fluorescence imaging/spectroscopy analyses of single HEWL crystals, primarily hexagonal ones, were conducted under an inverted microscope (IX73, Olympus). A schematic drawing of the experimental setup is presented in Figure S2. After the dye solution was injected into the crystal solution, the crystallization plate was settled on the microscope. It was then illuminated with white light from a halogen lamp via a condenser lens (IX2-LWUCD, Olympus) for transmittance or with a 405 nm CW laser beam from a DPSS laser (MDL-III-405, CNI) via a 4× microscope objective lens (UPLFLN 4×, Olympus) for fluorescence excitation. To adjust the apparatus to the crystallization plate thickness, an optical height spacer was utilized under the objective (10 mm height, custom, Tokyo Instruments). The 405 nm laser beam radius in lateral was expanded to 500 μm at the focal plane by inserting an $f = 400$ mm lens in front of the microscope to illuminate the crystals uniformly. The laser intensity was set to 300 mW/cm². The transmission/fluorescence emission images were recorded using a CMOS camera (TrueChrome Metrics, Tucson Photonics). For the spectroscopic measurements, the light was spatially selected using an imaging pinhole (250 μm radius) and sent to a polychromator (DU420A-BVS, Andor) coupled to a CCD camera (SR303i-A, Andor). The spatial resolution of the spectroscopic measurement was determined as roughly 5 μm in lateral and 20 μm in vertical.

RESULTS AND DISCUSSION

In the first instance, we demonstrated the incorporation of the dye molecule into HEWL crystals using stereoscopic microscopy, as presented in Figure 2. In this experiment, 400 μM of the eosin Y solution was injected into the crystal mother solution, and the temporal change was observed in a single well of the crystallization plate. As can be seen, some small HEWL crystals were visible in the mother solution in the single well. Moreover, the solution was red due to the presence of eosin Y

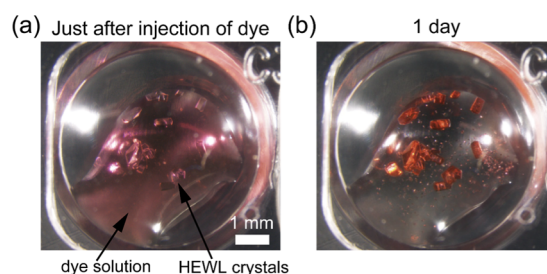


Figure 2. Stereoscopic microscopic images of a single well of a 48-well crystallization plate containing already-grown hen egg-white lysozyme (HEWL) crystals with the mother solution immediately after injection of 400 μM eosin Y solution into the (a) well and (b) 1 day after the injection.

(Figure 2a). After 24 h, the color of the solution changed to transparent, whereas the crystals appeared red (Figure 2b). Dissolution of the crystals was not observed. It is noteworthy that the HEWL crystals were originally transparent in the visible region, as presented in Figure 1a,b. This was also confirmed by the transmittance spectroscopy analysis of single crystals demonstrated in Figure S3. Thus, these outcomes indicate that the molecules of eosin Y were successfully captured inside the crystals in the solution, though such painting of cross-linked HEWL crystals upon dye incorporation was already reported.²¹ Recently, Mizra et al. have proposed that this dye incorporation into protein crystals can be used as a method to identify protein crystals from salt crystals,²⁵ so this demonstration would support their findings.

We subsequently studied the dye-loading process at a single-crystal level. We loaded the cationic dye, i.e., acridine yellow G, into the lysozyme crystals by the addition of a 400 μM dye solution into the mother solution. The temporal change of transmittance and fluorescence images obtained immediately after the injection up to 1 day is presented in Figure 3. It was not possible to distinguish the crystals from the solution instantaneously after the addition of acridine yellow G in both transmittance and fluorescence images (Figure 3a); however, with time, the crystals became brighter compared with the solution in the fluorescence images. On the other hand, the transmittance images were colored from transparent to pale yellow. It is noteworthy that the dark corners of the crystal indicate the refraction of light. The differential fluorescence image between the one obtained after 1 day and the one obtained immediately after the dye injection is presented in Figure 3b. It clearly visualizes that the concentration of acridine yellow G increased in the crystal compared with the surrounding.

Temporal changes of fluorescence intensity at specific points of both inside and outside of the crystal are summarized in Figure 3c. It is clear that the fluorescence intensity at the crystal inside increased with time, whereas the intensity at outside the crystal decreased. After 1 h, the intensity of the inside of the crystal saturated. This suggests that the molecules rapidly penetrated into the crystal (i.e., within 1 h). Furthermore, judging from the fluorescence intensity, the concentration of acridine yellow G was 1.7 times higher in the crystal than in the solution. Because the intensity drop after the saturation was not observed, we suppose that acridine yellow G molecules do not fully occupy the crystal and concentration or aggregation quenching does not occur in this condition. To confirm that the molecules penetrated the channels and did

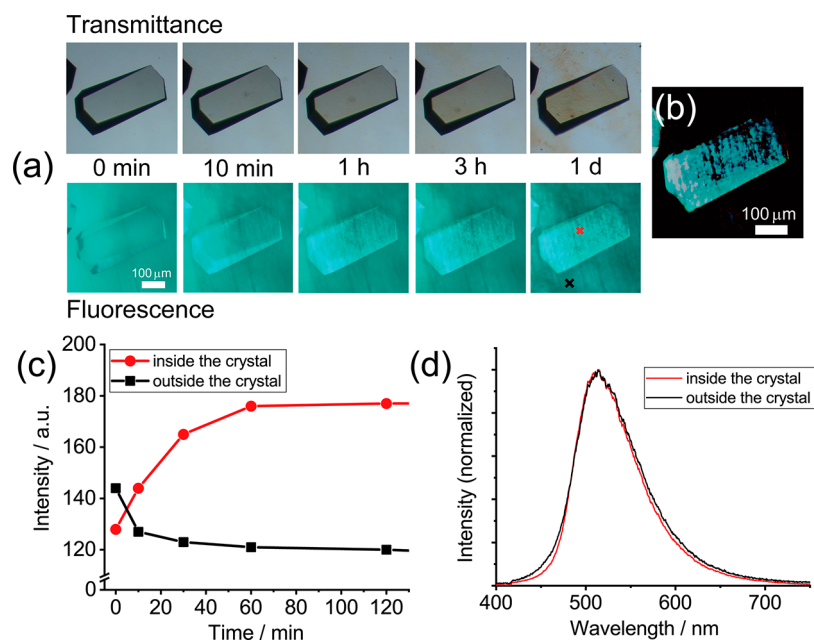


Figure 3. (a) Temporal change of transmittance and fluorescence images of a single HEWL crystal immediately after the injection of 400 μM acridine yellow G into the mother solution and up to 1 day following the injection. (b) Differential fluorescence image between the one obtained after 1 day and the one obtained immediately after the dye injection. (c) Temporal change of fluorescence intensity at inside (red) and outside (black) the crystal after the injection of acridine yellow G. The measured positions are indicated in image (a) (red and black crosses). (d) Space-resolved fluorescence spectra of the inside of a single HEWL crystal 1 day after acridine yellow G incorporation (red) and outside the crystal (black). The measured positions are indicated in image (a) (red and black crosses).

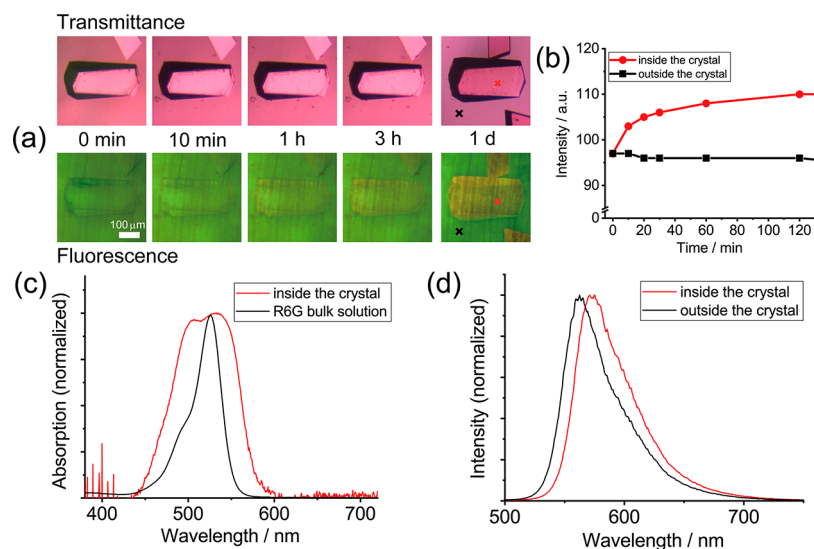


Figure 4. (a) Temporal changes of the transmittance and fluorescence images of a single HEWL crystal obtained immediately after the injection of 400 μM rhodamine 6G into the mother solution and up to 1 day. (b) Temporal changes of fluorescence intensities at inside (red) and outside (black) the crystal after the injection of rhodamine 6G. The measured positions are indicated in image (a) (red and black crosses). (c) Temporal changes of fluorescence intensity at inside (red) and outside (black) the crystal after the injection of rhodamine 6G. (d) Space-resolved absorption spectrum of the inside of a single HEWL crystal following rhodamine 6G incorporation (red). The spectrum was taken from the indicated position in image (a) (red cross). For comparison, an absorption spectrum of a 10 μM rhodamine 6G sodium acetate buffer solution is also shown (black). (e) Space-resolved fluorescence spectra of the inside of a single HEWL crystal 1 day after rhodamine 6G incorporation (red) and of the outside of the crystal (black). The measured positions are indicated in image (a) (red and black crosses).

not adsorb only on the crystal surface, we crushed the crystals using a glass rod to form fragments and observed their fluorescence. Based on this analysis, we concluded that the molecules penetrated into the HEWL crystals. Additionally, we also found that the crystals, into which acridine yellow G penetrated, did not exhibit any cracks and deformations; hence, we deduced that the molecules were loaded via the

solvent channels. We could not observe penetration anisotropy; however, the crystals possess a three-dimensional anisotropic solvent channel network. Detailed investigation at the early stage of the dye loading would be necessary to elucidate this.

The penetration time of acridine yellow G into the HEWL crystals was relatively short compared with that in the previous

reports. Cvetkovic et al. described that the xanthene dye uptake from 26 μM solution into the cross-linked HEWL crystals occurred over 2–10 days until reaching equilibrium, which was confirmed by ultraviolet (UV)–visible spectroscopy of the crystal suspensions.¹⁶ Seemann et al. also confirmed pH-sensitive xanthene dye loading into single cross-linked HEWL crystals after 72 h of incubation in the bath solution (100 μM) with two-photon microscopy.²¹ This disparity of the penetration time can be explained in terms of the size relationship between the molecules and pores. Tetragonal HEWL crystals contain semielliptical solvent channels along their *c*-axis (Figure 1c,d), the size of which is approximately 2.2 nm in the short axis.¹ On the other hand, acridine yellow G is a rodlike molecule with sizes of approximately 0.3 and 1.0 nm in short and long axes, respectively. These dimensions are therefore considerably smaller than the pore size, resulting in faster diffusion into the pore compared with the xanthene dye. In addition, the flexibility of the native crystals also results in the fast penetration compared with rigid cross-linked crystals. We speculate that the driving force for the molecular loading into the protein nanopores is the capillary condensation²⁶ based on the van der Waals force due to the large surface area of the pores. Following loading of the dye into the HEWL crystals, we replaced the dye buffer solution surrounding the crystals with a solution without the dye. We found that the dye molecules did not diffuse back to the surroundings from the pores for several hours. It is supposed that the dye molecules weakly bind to the pore surface as a consequence of van der Waals forces. This irreversibility of loaded molecules in the solvent channels was also confirmed in the following experiments.

Concurrently, we recorded the fluorescence spectrum of the inside and the outside of the crystal, as presented in Figure 3d; however, there was no difference between the spectra. This implies that the conditions of acridine yellow G loaded into the crystal are analogous to those in the solution. Nonetheless, the concentration in the crystal is higher than that in the solution. To support this assumption, we established that the fluorescence image of the HEWL crystal containing acridine yellow G did not exhibit any change with respect to rotating the polarization axis of the excitation light. We assume that acridine yellow G randomly oriented in the pores because of the availability of a relatively large space, considering the size of the molecule and, consequently, reduced interaction with the pore surface.

We subsequently investigated the incorporation of another dye, namely, rhodamine 6G, into single HEWL crystals. This cationic fluorescent molecule belongs to the xanthene dyes and was loaded analogously to acridine yellow G, i.e., by the addition of a 400 μM solution of the dye into the mother solution. The temporal change of transmittance and fluorescence images in this experiment is presented in Figure 4. Following the injection of the dye, we observed bright-green fluorescence in the entire image due to the presence of rhodamine 6G, and it was not possible to distinguish between the crystal and solution. In contrast to the experiments with acridine yellow G, in this case, the crystal gradually turned red on the edges. Notably, the red emission in the crystal is different from that of the rhodamine 6G solution, implying a change of the molecule conditions in the channels. Eventually, the entire crystal turned red; however, the emission intensity appeared weaker than that observed for acridine yellow G. On the other hand, the time course of the transmittance images

did not exhibit drastic changes, though the color of the solution slightly faded. This minor change in the transmittance images is probably due to a high absorption coefficient and reduced incorporation of rhodamine 6G. The temporal change of fluorescence intensity in Figure 4b indicates that the intensity at the crystal inside increased and that at the outside decreased with time and the changes saturated within 2 h. This behavior is similar to the case in acridine yellow G injection; however, the changes in intensity are less, supporting the reduced incorporation of rhodamine 6G.

To obtain further insight into the presence of rhodamine 6G in the solvent channels, we recorded the absorption and fluorescence spectra after 1 day of incubation. The absorption spectrum of the HEWL crystal at specific points is demonstrated in Figure 4c. As can be seen, the absorption spectrum of the bulk solution exhibits a single peak at approximately 525 nm as well as a vibronic shoulder at a lower wavelength (~ 500 nm), suggesting the presence of a monomeric form of rhodamine 6G. In contrast, the absorption spectrum of the inside of the crystal is broadened compared with that of the solution, and two peaks at approximately 505 and 532 nm can be observed. These can be assigned to H-type and J-type dimers of rhodamine 6G, respectively.²⁷ Furthermore, the fluorescence spectrum inside the crystal (Figure 4d) shows a peak at around 573 nm, which is red-shifted compared with the solution, supporting the red emission in the fluorescence images. This red-shifted fluorescence can be assigned to the fluorescent J-type dimers, whereas H-type dimers are nonfluorescent. Accordingly, the formation of rhodamine 6G aggregates in the solvent channels of the HEWL crystals upon incorporation is suggested. Disordered and twisted H-type dimers, in which the distortion angle between the dipole moments of the two monomers is higher than 55° , would be produced in the channels, resulting in the compatibility of the spectroscopic properties of the H-type and J-type dimers.²⁸ The formation of aggregates is often reported in the case of incorporation of rhodamine 6G into confined environments, such as clay thin films^{29,30} or mesostructured silica films.³¹

The temporal change of the emission color in Figure 4a shows that the red emission indicating rhodamine 6G aggregation was initially observed at the edge of the crystal and gradually reached the center. We followed the temporal change of the fluorescence spectrum at the center of the crystal upon loading of rhodamine 6G and found that the peak position shifted to a longer wavelength with incubation time (Figure S4). Thus, we assume that the rhodamine 6G molecules are incorporated into the crystal as monomers, and the subsequent penetration induces aggregation in the channels from the edge, probably by pushing away the already-adsorbed molecules. This assumption was partially confirmed by the fluorescence spectrum of the surrounding solution, which was ascribed to the monomeric form of rhodamine 6G at this concentration (Figure 4d). Lastly, we concluded that the rhodamine 6G aggregates were formed in the solvent channels, suggesting their chemically heterogeneous environments. It is noteworthy that this aggregation formation of loaded molecules in the protein crystals is not found in previous reports, probably due to the relatively lower amount of loaded molecules compared with that in this experiment.

According to the previous studies concerning the separation of dyes using mesoporous silica, nanoporous materials are discussed in terms of the Langmuir isotherm model.³² The

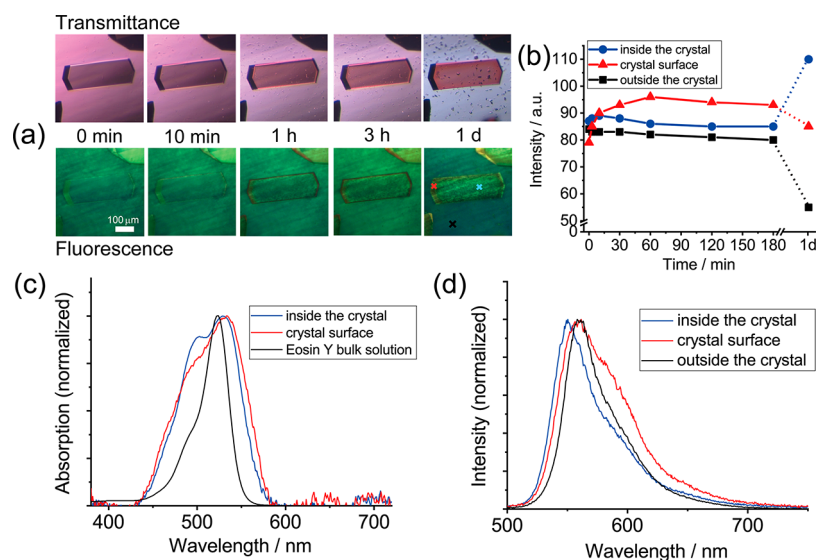


Figure 5. (a) Temporal changes of the transmittance and fluorescence images of a single HEWL crystal obtained immediately after injection of 400 μM eosin Y into the mother solution and up to 1 day. (b) Temporal changes of fluorescence intensity at inside (blue) and outside (black) the crystal and the surface (red) after the injection of eosin Y. The measured positions are indicated in image (a) (blue, red, and black crosses). (c) Space-resolved absorption spectrum of the inside of a single HEWL crystal following eosin Y incorporation (red). The spectrum was taken from the position indicated in image (a) (blue and red crosses). For comparison, the absorption spectrum of a 10 μM eosin Y sodium acetate buffer solution is also shown (black). (d) Space-resolved fluorescence spectra of the inside and the surface of a single HEWL crystal 1 day after eosin Y incorporation (blue and red) and outside of the crystal (black). The measured positions are indicated in image (a) (blue, red, and black crosses).

model is based on the assumption that the monolayer coverage of the adsorbed molecules occurs over homogeneous sites, and a saturation point is reached when no further adsorption can take place. We examined the concentration dependence on the fluorescence spectra of single HEWL crystals upon rhodamine 6G loading (Figure S5) and found that the peak position shifted to a longer wavelength with increasing concentration; however, its saturation was not observed. It is assumed that the coverage of rhodamine 6G on the channel surface is not complete, and a quantitative analysis of the adsorbed amount will be conducted in the near future. From this viewpoint, it is important to remember that the molecules of rhodamine 6G are positively charged. HEWLs are highly protonated in the acidic buffer (pH = 4.5) below the isoelectric point (pH = 9.3), and the channel surface possesses more positively charged sites than negatively charged ones. Inside the channel is rich in counterions of the sites, and then the molecular incorporation occurs by replacing the molecules with the ions and binding onto the oppositely charged sites to the molecules. Therefore, binding sites of rhodamine 6G would be limited, resulting in less incorporation. Moreover, the electrostatic repulsive interaction between rhodamine 6G and the oppositely charged site in the channel may induce the aggregation. Ultimately, we propose that the incorporation behavior of rhodamine 6G into the HEWL crystals, including the enhancement of the molecular aggregation in the channels, could be considered to be a host–guest interaction in protein crystals as nanoporous materials.

For comparison of the rhodamine 6G incorporation, we introduced another xanthene dye, namely, eosin Y, the absorption and fluorescence spectra of which are nearly identical to those of rhodamine 6G, as presented in Figure S6. However, eosin Y molecules are anionic and therefore contain opposite charges to rhodamine 6G. Nevertheless, both of the molecules are incorporated into single HEWL crystals in the same manner. The temporal change of the optical images is

summarized in Figure 5a. In the time course of the fluorescence images, it is obvious that the crystal edge in the emission images gradually turned from green to red after 1 h of incubation and the boundary appeared clear. As is the case with rhodamine 6G, the green and red emissions correspond to the monomer and the fluorescent J-type dimer of eosin Y, respectively. The red emission area did not expand with time in contrast to the case of rhodamine 6G. On the other hand, the emission color inside the crystal kept green but the brightness seems not so different from the solution after 3 h of incubation. The fluorescence image after 1 day of incubation shows that the crystal became brighter than the solution, whereas the red emission from the edge became weaker. Considering the vivid contrast between the crystal and the surrounding in both the transmittance and fluorescence images after 1 day, we assume that the HEWL crystals can occlude more of the eosin Y molecules than of rhodamine 6G. Cvetkovic et al. examined the adsorption isotherms of several kinds of xanthene dyes in cross-linked tetragonal HEWL crystals.¹⁶ They explained the differences in the affinities of the crystals in terms of the electrostatic interactions. Due to the presence of a negative charge in eosin Y, our assumption is also supported by their findings. Temporal changes of fluorescence intensity at specific positions in Figure 5a are summarized in Figure 5b. Different from the experiment in rhodamine 6G, the intensities inside and outside the crystal change little with time. Contrastingly, the intensity at the crystal edge increases with time and saturates after 1 h of incubation. Judging from the fluorescence image after 1 day of incubation, it is plausible that the loading of eosin Y into the crystal inside is followed by the appearance of red emission at the crystal edge, implying the eosin Y dimer formation. Thus, the incorporation of eosin Y into the HEWL crystals is considered to take place in two steps. First, the dimer forms on the surface, and second, the monomer is loaded into the crystal. This process is substantially different

from the case with rhodamine 6G and would be caused by the host–guest interaction in protein crystals.

The absorption and fluorescence spectra of the HEWL crystals after 1 day of incubation with the eosin Y solution are presented in Figure 5c,d. Similarly to the case of the incorporation of rhodamine 6G, the absorption spectra of both the inside and the surface of the crystal are broadened compared with those of the solution and show two peaks at around 500 and 530 nm. Consequently, it is suggested that eosin Y forms H-type and J-type dimers in both the channel and at the crystal surface. It should be mentioned that the spectrum of the crystal surface is slightly broader than that of the inside of the crystal, and the H-aggregate component is reduced, suggesting that the distortion angle between the dipole moments of eosin Y is different. On the other hand, the fluorescence spectrum of the inside of the crystal shows a peak at around 550 nm, which is blue-shifted compared with that of the surrounding solution. This blue shift may be explained in terms of not only electrostatic interaction but also the hydrophilicity of eosin Y. It is reported that incorporation of a halogen into eosin Y increases the hydrophobicity compared to rhodamine 6G,³³ which can induce interactions with the hydrophilic proteins at the pore surface and result in a blue fluorescence shift. A similar blue shift has been reported for Nile red on the protein surface.³⁴ Hence, this interaction can be considered as a host–guest interaction, despite being different from the one described for rhodamine 6G.

In contrast to the inside of the crystal, the fluorescence spectrum of the crystal surface exhibits a broad shoulder at around 600 nm, in addition to the monomeric emission at 560 nm. Owing to the spatial resolution of the spectroscopic measurement ($\sim 5 \mu\text{m}$), the spectrum may contain contributions from both the crystal surface and the solution. Therefore, the monomeric emission is ascribed to the solution, and the shoulder corresponds to the crystal surface, which is in accordance with the red emission in the fluorescence image. The red-shifted fluorescence at the shoulder compared with the solution can be assigned to the emission of the eosin Y dimer; hence, the aggregation of eosin Y at the crystal surface was confirmed. This assumption is also supported by the fact that the red emission at the crystal edge was only observed in the case of incubation of the crystals in the eosin Y solution with a high concentration (Figure S7). The entry of many molecules of the dye into the crystals in a high-concentration solution results in the formation of aggregates, followed by monomer incorporation.

It is noteworthy that the eosin Y aggregates are mainly formed at the entry hole of the solvent channels. The fluorescence image (Figure 5a) clearly shows that the red emission is observed only at the edges of the crystal and not the (110) faces of the crystal. Additionally, another crystal incubated in a solution of eosin Y using an analogous approach shows red emission in the entire (101) face (Figure 6). This finding provides direct evidence that the molecules are transported into the crystal via the (101) face and thus via the solvent channels along the *c*-axis. Moreover, it shows that the aggregates are formed at the entry of the channels. It has previously been reported that the diffusion coefficient of loaded molecules in the HEWL crystals decreases due to the van der Waals forces and electrostatic interactions.¹⁸ Hence, clogging of molecules can occur at the entry. In addition, in the case of eosin Y, the electrostatic interactions are expected to be stronger due to the electrostatic attractive interaction between

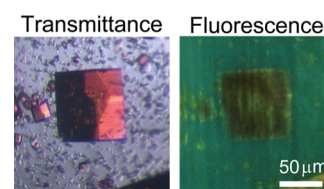


Figure 6. Transmittance and fluorescence images of a single HEWL crystal, which directs the (101) face to the top side 1 day after injection of $400 \mu\text{M}$ eosin Y into the mother solution.

eosin Y and the HEWLs. Thus, the binding would be stronger, leading to the aggregation at the entry. Moreover, the heterogeneous alignment of amino acid residues near the entry is suspected of playing an important role in the induction of aggregation. Thereafter, the formed aggregation at the entry can release the molecule, leading to the monomer incorporation into the crystal inside as confirmed by the fluorescence image (Figure 5a). Therefore, the aggregation of eosin Y at the entry holes of the solvent channels could be considered as another host–guest interaction in nanoporous protein crystals and is dependent on the molecular charge.

The dynamic process of the molecular incorporation into the HEWL crystals proposed on the basis of our observations for xanthene molecules is schematically summarized in Figure 7. Undoubtedly, this molecular incorporation process is

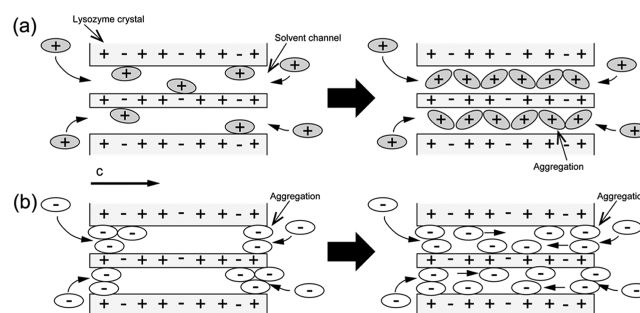


Figure 7. Schematic illustration of the molecular incorporation process into a HEWL crystal along the *c*-axis in the case of (a) cationic molecules (rhodamine 6G) and (b) anionic molecules (eosin Y).

strongly dependent on many factors related to the molecular and crystal properties; therefore, our proposal cannot be generalized. For instance, the behavior of acridine yellow G incorporation is different from that of rhodamine 6G, despite both molecules being cationic. On the other hand, we demonstrated that the molecular aggregation occurs upon molecular incorporation into the protein pores. This finding clearly suggests that the in situ observation not just by microscopic imaging but also using spectroscopy at a single-crystal level is necessary to thoroughly study the process. The overview of the molecular incorporation process into the protein crystal will be updated in the near future on the basis of systematic loading of molecules with varying molecular sizes, shapes, and charges.

CONCLUSIONS

In conclusion, we successfully performed in situ microspectroscopy observation of the fluorescent dye diffusion process into the HEWL crystals at a single-crystal level. We clearly visualized the molecule-loading process as a function of

time via transmittance and emission images of the crystal and spectroscopically clarified that the molecular incorporation process requires two steps. The first step is driven by the capillary condensation based on the van der Waals forces, whereas the second step involves the attractive or repulsive interactions of the molecules with the amino acid residues at the channel surface. These depend on the molecular charge and were shown to lead to molecular aggregation inside or at the surface of the crystal. Dye molecule accumulation in protein crystals has been 3D-reconstructed with confocal fluorescence or two-photon microscopy before;^{17,18,21} however, we in particular spectroscopically demonstrated the host–guest interaction that can come up to the surface by loading a large amount of molecules despite the lower spatial resolution of the microscopy. Further evaluation of the spatial arrangement of the amino acid residues at the surface of the solvent channels would allow for the elucidation of the role of the electrostatic interactions. Moreover, a comparison of the result obtained in the native HEWL crystals with cross-linked ones is also important because the stability of the cross-linked crystals could result in different behaviors. Further observation utilizing the confocal fluorescence microscopy technique would enable the visualization of the three-dimensional molecule-loading process with the crystal thickness, resulting in the quantitative evaluation of the amount of the loaded molecules. From the viewpoint of materials science, protein crystals can be applied as molecular sieves, as demonstrated in this study. Considering the structural similarity to the metal–organic frameworks and the variety of proteins, they can be further developed for applications in gas separation, catalysis, and nanoreactors. In addition, we propose that the crystals occluding dye molecules can be regarded as novel optical materials, as the guest molecules are highly condensed in the three-dimensional solvent channels. In this sense, the finding by Higger's group,³⁵ which showed that rhodamine 6G aggregates arranged on amyloid fibrils of HEWL exhibit stimulated emission, suggests potential applications of the protein crystals in biolasers because the molecular arrangement in the solvent channels possesses a more highly ordered structure compared with the fibrils.

■ ASSOCIATED CONTENT

Supporting Information

The Supporting Information is available free of charge at <https://pubs.acs.org/doi/10.1021/acsomega.0c01038>.

a- and *b*-axis projections of the structure of a tetragonal hen egg-white lysozyme crystal; schematic illustration of the optical measurement setup; transmittance spectrum of a single hen egg-white lysozyme crystal; temporal change of the fluorescence spectrum of the inside of a single hen egg-white lysozyme crystal upon rhodamine 6G loading; concentration dependence of the fluorescence spectrum of the inside of a single hen egg-white lysozyme crystal upon rhodamine 6G loading; absorption and fluorescence spectra of 10 μ M rhodamine 6G and eosin Y solution; and concentration dependence of transmittance and fluorescence images of a single hen egg-white lysozyme crystal upon eosin Y incorporation (PDF)

■ AUTHOR INFORMATION

Corresponding Author

Takayuki Uwada – Department of Chemistry, Josai University, Sakado 350-0295, Japan; orcid.org/0000-0003-4272-7964; Phone: +81-49-271-7996; Email: uwada@josai.ac.jp

Authors

Kohei Kouno – Department of Chemistry, Josai University, Sakado 350-0295, Japan

Mitsuru Ishikawa – Department of Chemistry, Josai University, Sakado 350-0295, Japan

Complete contact information is available at: <https://pubs.acs.org/10.1021/acsomega.0c01038>

Author Contributions

T.U. conceived and designed the experiment. T.U. and K.K. performed sample preparation and the optical measurements. T.U. analyzed the data and wrote the manuscript with contributions from all authors. All authors have given approval to the final version of the manuscript.

Notes

The authors declare no competing financial interest.

■ ACKNOWLEDGMENTS

This work was supported by JSPS KAKENHI (Grant No. 16K21325) to T.U. Research funding at Josai University to T.U. is also acknowledged. The authors thank Prof. Kaori Sano from Josai University for the stereoscopic microscope observations.

■ REFERENCES

- (1) Abe, S.; Maity, B.; Ueno, T. Design of a Confined Environment Using Protein Cages and Crystals for the Development of Biohybrid Materials. *Chem. Commun.* **2016**, *52*, 6496–6512.
- (2) Vilenchik, L. Z.; Griffith, J. P.; Clair, N.; Navia, M. A.; Margolin, A. L. Protein Crystals as Novel Microporous Materials. *J. Am. Chem. Soc.* **1998**, *120*, 4290–4294.
- (3) Margolin, A. L.; Navia, M. A. Protein Crystals as Novel Catalytic Materials. *Angew. Chem., Int. Ed.* **2001**, *40*, 2204–2222.
- (4) Brühwiler, D.; Calzaferri, G.; Torres, T.; Ramm, J. H.; Gartmann, N.; Dieu, L.-Q.; López-Duarte, I.; Martínez-Díaz, M. V. Nanochannels for Supramolecular Organization of Luminescent Guests. *J. Mater. Chem.* **2009**, *19*, 8040–8067.
- (5) Wan, Y.; Zhao. On the Controllable Soft-Templating Approach to Mesoporous Silicates. *Chem. Rev.* **2007**, *107*, 2821–2860.
- (6) Chen, L.; Luque, R.; Li, Y. Controllable Design of Tunable Nanostructures inside Metal–Organic Frameworks. *Chem. Soc. Rev.* **2017**, *46*, 4614–4630.
- (7) Lopez, S.; Rondot, L.; Leprêtre, C.; Marchi-Delapierre, C.; Ménage, S.; Cavazza, C. Cross-Linked Artificial Enzyme Crystals as Heterogeneous Catalysts for Oxidation Reactions. *J. Am. Chem. Soc.* **2017**, *139*, 17994–18002.
- (8) Tabe, H.; Fujita, K.; Abe, S.; Tsujimoto, M.; Kuchimaru, T.; Kizaka-Kondoh, S.; Takano, M.; Kitagawa, S.; Ueno, T. Preparation of a Cross-Linked Porous Protein Crystal Containing Ru Carbonyl Complexes as a Co-Releasing Extracellular Scaffold. *Inorg. Chem.* **2015**, *54*, 215–220.
- (9) Muskens, O. L.; England, M. W.; Danos, L.; Li, M.; Mann, S. Plasmonic Response of Ag- and Au-Infiltrated Cross-Linked Lysozyme Crystals. *Adv. Funct. Mater.* **2013**, *23*, 281–290.
- (10) Guli, M.; Lambert, E. M.; Li, M.; Mann, S. Template-Directed Synthesis of Nanoplasmonic Arrays by Intracrystalline Metalization of Cross-Linked Lysozyme Crystals. *Angew. Chem., Int. Ed.* **2010**, *49*, 520–523.

- (11) England, M. W.; Patil, A. J.; Mann, S. Synthesis and Confinement of Carbon Dots in Lysozyme Single Crystals Produces Ordered Hybrid Materials with Tuneable Luminescence. *Chem. – Eur. J.* **2015**, *21*, 9008–9013.
- (12) Abe, S.; Tsujimoto, M.; Yoneda, K.; Ohba, M.; Hikage, T.; Takano, M.; Kitagawa, S.; Ueno, T. Porous Protein Crystals as Reaction Vessels for Controlling Magnetic Properties of Nanoparticles. *Small* **2012**, *8*, 1314–1319.
- (13) Zhang, Y.; Zhang, X.; Tang, J.; Snow, C. D.; Sun, G.; Kowalski, A. E.; Hartje, L. F.; Zhao, N.; Wang, Y.; Belfiore, L. A. Synthesis of Luminescent Lanthanide Complexes within Crosslinked Protein Crystal Matrices. *CrystEngComm* **2018**, *20*, 2267–2277.
- (14) Farhadian, N.; Malek, K.; Shariaty-Niassar, M.; Maghari, A. Glycine Amino Acid Transport inside the Nanopores of Lysozyme Protein Crystal. *Chem. Lett.* **2011**, *40*, 1420–1422.
- (15) Guli, M.; Li, M.; Hu, Z.; Yao, J.; Mann, S. Fabrication of Photoluminescent Hybrid Protein Crystals of Lysozyme and Bromophenol Blue. *J. Mater. Sci.* **2015**, *50*, 7026–7030.
- (16) Cvetkovic, A.; Straathof, A. J. J.; Krishna, R.; van der Wielen, L. A. M. Adsorption of Xanthene Dyes by Lysozyme Crystals. *Langmuir* **2005**, *21*, 1475–1480.
- (17) Cvetkovic, A.; Picioreanu, C.; Straathof, A. J. J.; Krishna, R.; van der Wielen, L. A. M. Quantification of Binary Diffusion in Protein Crystals. *J. Phys. Chem. B* **2005**, *109*, 10561–10566.
- (18) Cvetkovic, A.; Picioreanu, C.; Straathof, A. J. J.; Krishna, R.; van der Wielen, L. A. M. Relation between Pore Sizes of Protein Crystals and Anisotropic Solute Diffusivities. *J. Am. Chem. Soc.* **2005**, *127*, 875–879.
- (19) Cvetkovic, A.; Zomerdijk, M.; Straathof, A. J. J.; Krishna, R.; van der Wielen, L. A. M. Adsorption of Fluorescein by Protein Crystals. *Biotechnol. Bioeng.* **2004**, *87*, 658–668.
- (20) Mori, K.; Kuhn, B. Imaging Ca²⁺ Concentration and Ph in Nanopores/Channels of Protein Crystals. *J. Phys. Chem. B* **2018**, *122*, 9646–9653.
- (21) Seemann, K. M.; Kiefersauer, R.; Jacob, U.; Kuhn, B. Optical Ph Detection within a Protein Crystal. *J. Phys. Chem. B* **2012**, *116*, 9873–9881.
- (22) Li, M.; Nadarajah, A.; Pusey, M. L. Growth of (101) Faces of Tetragonal Lysozyme Crystals: Determination of the Growth Mechanism. *Acta Crystallogr., Sect. D: Biol. Crystallogr.* **1999**, *55*, 1012–1022.
- (23) Tsekova, D. S. Formation and Growth of Tetragonal Lysozyme Crystals at Some Boundary Conditions. *Cryst. Growth Des.* **2009**, *9*, 1312–1317.
- (24) Vaney, M. C.; Maignan, S.; Ries-Kautt, M.; Ducruix, A. High-Resolution Structure (1.33 Å) of a Hew Lysozyme Tetragonal Crystal Grown in the Apcf Apparatus. Data and Structural Comparison with a Crystal Grown under Microgravity from Spacehab-01 Mission. *Acta Crystallogr., Sect. D: Biol. Crystallogr.* **1996**, *52*, 505–517.
- (25) Mirza, S.; Akbar, Z.; Ahmad, M. S. A Simple Nondestructive, Cost-Effective Method for Differentiation of Protein Crystals from Salt Crystals by Using a Natural Dye. *Cryst. Growth Des.* **2019**, *19*, 3612–3615.
- (26) Ariga, K.; Vinu, A.; Ji, Q.; Ohmori, O.; Hill, J. P.; Acharya, S.; Koike, J.; Shiratori, S. A Layered Mesoporous Carbon Sensor Based on Nanopore-Filling Cooperative Adsorption in the Liquid Phase. *Angew. Chem., Int. Ed.* **2008**, *47*, 7254–7257.
- (27) del Monte, F.; Mackenzie, J. D.; Levy, D. Rhodamine Fluorescent Dimers Adsorbed on the Porous Surface of Silica Gels. *Langmuir* **2000**, *16*, 7377–7382.
- (28) del Monte, F.; Levy, D. Formation of Fluorescent Rhodamine B J-Dimers in Sol–Gel Glasses Induced by the Adsorption Geometry on the Silica Surface. *J. Phys. Chem. B* **1998**, *102*, 8036–8041.
- (29) Sasai, R.; Iyi, N.; Fujita, T.; Arbeloa, F. L.; Martínez; Takagi, K.; Itoh, H. Luminescence Properties of Rhodamine 6g Intercalated in Surfactant/Clay Hybrid Thin Solid Films. *Langmuir* **2004**, *20*, 4715–4719.
- (30) Martínez Martínez, V.; López Arbeloa, F.; Bañuelos Prieto, J.; Arbeloa López, T.; López Arbeloa, I. Characterization of Rhodamine 6g Aggregates Intercalated in Solid Thin Films of Laponite Clay. 1. Absorption Spectroscopy. *J. Phys. Chem. B* **2004**, *108*, 20030–20037.
- (31) Malfatti, L.; Kidchob, T.; Aiello, D.; Aiello, R.; Testa, F.; Innocenzi, P. Aggregation States of Rhodamine 6g in Mesoporous Silica Films. *J. Phys. Chem. C* **2008**, *112*, 16225–16230.
- (32) Huang, C.-H.; Chang, K.-P.; Ou, H.-D.; Chiang, Y.-C.; Wang, C.-F. Adsorption of Cationic Dyes onto Mesoporous Silica. *Microporous Mesoporous Mater.* **2011**, *141*, 102–109.
- (33) Majima, E.; Yamaguchi, N.; Chuman, H.; Shinohara, Y.; Ishida, M.; Goto, S.; Terada, H. Binding of the Fluorescein Derivative Eosin Y to the Mitochondrial Adp/Atp Carrier: Characterization of the Adenine Nucleotide Binding Site. *Biochemistry* **1998**, *37*, 424–432.
- (34) Sackett, D. L.; Wolff, J. Nile Red as a Polarity-Sensitive Fluorescent Probe of Hydrophobic Protein Surfaces. *Anal. Biochem.* **1987**, *167*, 228–234.
- (35) Hanczyc, P.; Sznitko, L.; Zhong, C.; Heeger, A. J. Stimulated Emission from Rhodamine 6g Aggregates Self-Assembled on Amyloid Protein Fibrils. *ACS Photonics* **2015**, *2*, 1755–1762.